

The 3a Accessory Protein of SARS Coronavirus Specifically Interacts with the 5'UTR of Its Genomic RNA, Using a Unique 75 Amino Acid Interaction Domain[†]

Kulbhushan Sharma,[‡] Milan Surjit,[‡] Namita Satija,[‡] Boping Liu,[§] Vincent T. K. Chow,[§] and Sunil K. Lal^{*,‡}

Virology Group, International Centre for Genetic Engineering & Biotechnology, Aruna Asaf Ali Road, New Delhi 110067, India, and Microbiology Department, National University of Singapore, Singapore

Received October 3, 2006; Revised Manuscript Received April 3, 2007

ABSTRACT: More than four years have passed since the outbreak of the severe acute respiratory syndrome (SARS) epidemic, and still very little is known about the molecular biology and pathogenesis of this deadly virus. Among the accessory proteins of the SARS coronavirus (SARS-CoV), the 3a protein has been shown to interact with the spike, envelope, and membrane glycoprotein and has recently been established to be a structural component of capsid. Recent studies suggest that the 3a protein may function as an ion channel and may promote virus release. In order to further characterize the functional properties of this protein, we initiated studies to check its RNA binding activity. Using the yeast three-hybrid system, electrophoretic mobility shift assay (EMSA), and ultraviolet (UV) cross-linking techniques, we have shown that the 3a protein is capable of binding specifically to the 5' untranslated region (5'UTR) of the SARS virus genomic RNA. Further, we have mapped the interaction domain of the 3a protein responsible for this RNA–protein interaction using a series of deletion mutants and defined it to the central 75 amino acid region. This RNA binding motif of 3a does not share homology with any other known RNA binding protein and may have an important role in viral capsid assembly and pathogenesis.

The virus responsible for severe acute respiratory syndrome (SARS¹) is a novel human coronavirus (SARS-CoV) that has become a serious public health concern since its identification after the epidemic in 2003 which resulted in more than 8400 cases and around 800 deaths in different regions of the world (1–3). SARS-CoV is an enveloped, positive-stranded RNA virus comprising approximately 30,000 nucleotides. Like other members of the genus coronavirus, e.g., murine hepatitis virus (MHV) and bovine coronavirus (BCoV), the SARS-CoV genome contains six major open reading frames (ORFs) that encode the two replicase polyprotein and four structural proteins such as the spike (S) glycoprotein, the envelope (E) protein, the membrane (M) glycoprotein, and the nucleocapsid (N) protein (1, 2, 4, 5). Earlier studies indicate SARS-CoV to be different from other coronaviruses and constitute a fourth group in the *Coronavirus* genus (2, 3, 6, 7). However, many studies have identified the group 2 coronaviruses as the closest relatives of SARS-CoV (8–11). In contrast to other human coronaviruses that cause benign infection such as common cold, SARS-CoV is highly virulent and induces acute atypical pneumonia associated with a high mortality rate (~3–6%)

that is even higher (~43–55%) in the elderly population (6). Therefore, it is critical from both medical and research points of view to find out the factors that enable SARS-CoV to behave so distinctly from other human coronaviruses.

Apart from its divergence from other coronaviruses in amino acid sequence of other known structural proteins, the SARS-CoV also possesses nine unique ORFs that encode accessory proteins. Given that these proteins are novel in nature and uniquely present only in the SARS-CoV genome, it is tempting to speculate that they might be playing a significant regulatory role during viral pathogenesis. However, to date only the 7a, 6, and 3a proteins have been studied to some extent (3, 12–20).

The 3a protein (also termed as X1 or U274) is translated from the ORF3 of the SARS-CoV genome (Figure 1A). It is the largest of all predicted SARS-CoV accessory proteins consisting of 274 amino acids (3) and lacks significant homology with any other known protein, although some regions show low-level homology to cytochrome b561, outer membrane porin of bacteria, and the calcium pump of malaria parasite (19). This protein has been experimentally demonstrated to be expressed in SARS-CoV infected patients as well as in VeroE6 cells infected with SARS-CoV using immunohistochemistry and immunofluorescence assays (19). Sera from SARS patients could detect recombinant 3a protein expressed in *Escherichia coli*, further proving that this protein is indeed expressed during the SARS-CoV life cycle (19). 3a is a type III membrane protein that associates with the viral membrane and is distributed over the cytoplasm in a fine punctate pattern (19). An elegant study done by Tan et al. has shown that this protein gets transported to the

[†] This work was supported by internal funds from the International Centre for Genetic Engineering & Biotechnology, New Delhi, and a research grant on SARS from the Department of Biotechnology to S.K.L.

* Corresponding author. E-mail address: sunillal@icgeb.res.in.

[‡] International Centre for Genetic Engineering & Biotechnology.

[§] National University of Singapore.

¹ Abbreviations: SARS, severe acute respiratory syndrome; UTR, untranslated region; ORF, open reading frame; aa, amino acids; nt, nucleotides; AD, activation domain; BD, binding domain; 3-AT, 3-amino-1,2,3-triazole.

Table 1: Yeast Strains, Plasmids, Recombinant Plasmid Constructs and Primers Used in This Study

| strain/plasmid/ construct/primers | genotype/description |
|--------------------------------------|--|
| | Strains |
| L40-coat | MATa, ura3-52 leu2-3, 112, his3Δ200, trp1Δ1, ade2, LYS2::(LexA-op)-His3, ura3::(LexA-op)-LacZ, LexA-MS2 coat (TRP1) |
| | Plasmids |
| pGAD pIII/MS2-1, 2 | GAL4 AD vector [GAL4 (768–881)]; LEU2, 2 μm, Ampr derived from pIIIEx426RPR |
| | Constructs |
| pGAD-3a | SARS-3a cloned into pGEMTeasy vector using F1 R1 primers; pGEMTeasy-3a digested with <i>EcoRI</i> , Klenow treated, and cloned into <i>SmaI</i> site in pGAD |
| pGAD-3a (1–124) | 3a (1–372 bp) PCR amplified using F2 R2 primers cloned into pCR-XL-TOPO vector; pCR-XL-TOPO 3a (1–372 bp) digested with <i>SmaI</i> and <i>EcoRI</i> , fragment religated into pGAD at <i>SmaI</i> – <i>EcoRI</i> site |
| pGAD-3a (125–275) | 3a (373–825 bp) PCR amplified using F3 R3 primers and cloned into pCR-XL-TOPO vector; pCR-XL-TOPO 3a (373–825 bp) digested with <i>SmaI</i> and <i>EcoRI</i> , fragment religated into pGAD at <i>SmaI</i> – <i>EcoRI</i> site |
| pGAD-3a (125–200) | 3a (373–600 bp) PCR amplified using F3 R4 primers and cloned into pCR-XL-TOPO vector; pCR-XL-TOPO 3a (373–600 bp) digested with <i>SmaI</i> and <i>EcoRI</i> , fragment religated into pGAD at <i>SmaI</i> – <i>EcoRI</i> site |
| pGAD-3a (201–275) | 3a (601–825 bp) PCR amplified using F4 R3 primers and cloned into pCR-XL-TOPO vector; pCR-XL-TOPO 3a (601–825 bp) digested with <i>SmaI</i> and <i>EcoRI</i> , fragment religated into pGAD at <i>SmaI</i> – <i>EcoRI</i> site |
| pGAD-3a (1–70) | 3a (1–210 bp) PCR amplified using F2 R5 primers and cloned into pCR-XL-TOPO vector; pCR-XL-TOPO 3a (1–210 bp) digested with <i>SmaI</i> and <i>EcoRI</i> , fragment religated into pGAD at <i>SmaI</i> – <i>EcoRI</i> site |
| pGAD-3a (70–124) | 3a (210–372 bp) cloned into pCR-XL-TOPO by PCR using F5 R2 primers; pCR-XL-TOPO 3a (210–372 bp) digested with <i>SmaI</i> and <i>EcoRI</i> , fragment religated into pGAD at <i>SmaI</i> – <i>EcoRI</i> site |
| pCR-XL-TOPO-5'UTR | 1–264 bp fragment PCR amplified using F6 R6 primers and cloned into pCR-XL-TOPO vector using TA overhang ligation |
| pCR-XL-TOPO-3'UTR | 29389–29751 bp fragment PCR amplified using F7 R7 primers and cloned into pCR-XL-TOPO vector using TA overhang ligation |
| pIIIMS2-5'UTR | pCR-XL-TOPO-5'UTR digested with <i>SmaI</i> and cloned into <i>SmaI</i> site in pIII MS2-2 |
| pIIIMS1-3'UTR | pCR-XL-TOPO-3'UTR digested with BamHI, Klenow, then digested by <i>EcoRV</i> and cloned into <i>SmaI</i> site in pIII MS2-1 |
| | Primer Sequences: ^a |
| | F1: 5' CGAATTCATGGATTTGTTTATGAGATTTTTTAC 3' |
| | F2: 5' GGAATTCATGGATTTGTTTATGAGATTTTTT 3' |
| | F3: 5' GGAATTCATGAGATGTTGGCTTTGTTGGAAGTGC 3' |
| | F4: 5' GGAATTCGTCGTTGTACATGGCTATTTACCGAA 3' |
| | F5: 5' GGAATTCCTAGCCCTTTATAAGGGCTTCCAGTTC 3' |
| | F6: 5' CCCGGGATATTAGGTTTTTACCTACCCAGG 3' |
| | F7: 5' CCCGGGCCATGAGTGGAGCTTCTG 3' |
| | R1: 5' CTGCAGTTACAAAGGCACGCTAGTAGTC 3' |
| | R2: 5' TCCCCCGGAATAATTCTACATGCGTT 3' |
| | R3: 5' TCCCCCGGTTACAAAGGCACGCTAGTAGT 3' |
| | R4: 5' TCCCCCGGATAGTCTTAAACACCTGAGTGCCT 3' |
| | R5: 5' TCCCCCGGGCTGCCATCTTTTTATT 3' |
| | R6: 5' TAGCATGCACACCCGGACGAAACCTA 3' |
| | R7: 5' CGGCATGCTTGTCATTCTCCTAAGAAGCTATT 3' |

^a F represents forward primer, and R represents reverse primer.

the yeast three-hybrid assay, electrophoretic mobility shift assay (EMSA), and UV-cross-linking assay, the 3a protein was found to interact with the 5' untranslated region (UTR) of the SARS-CoV genome. However, 3'UTR as well as a nonspecific RNA sequence (iron responsive element) failed to associate with the 3a protein, thus indicating that the 3a protein specifically associates only with the 5' region of the genome. Further, deletion mapping revealed that the central 75 amino acid (aa 125–200 from the N-terminus) region of the 3a protein was responsible for this RNA protein interaction. Interestingly, this region does not share homology with any other known RNA binding protein. Thus, we propose that the 3a protein contains a unique RNA binding motif. The possible significance of this RNA–protein interaction during the viral life cycle is discussed.

EXPERIMENTAL PROCEDURES

Plasmids and Reagents. Yeast strains and plasmid constructs used in this study are summarized in Table 1. The 3a region of SARS-CoV genome (GenBank accession number NC_004718; Figure 1A) was PCR amplified and cloned into the pGEMTeasy vector. In order to express N-terminal HA tagged 3a protein, pGEMTeasy-3a was digested with *EcoRI*, Klenow treated, and cloned into the *SmaI* site of pGAD vector (Figure 1C). All the deletions of 3a were PCR amplified using specific primers having sites for *SmaI* and *EcoRI* at the 5' and 3' ends respectively and were cloned into the pCR-XL-TOPO vector. These constructs were then digested with *SmaI*–*EcoRI*, and the fragment was ligated into pGAD vector and digested with the same set of enzymes.

SARS-CoV genomic sequence spanning 1–264nt from the 5' end (5'UTR) was PCR amplified and cloned into the pCR-XL-TOPO vector. The pCR-XL-TOPO-5'UTR was then digested with *SmaI* and *SphI* and was cloned into the *SmaI*–*SphI* site of pIII MS2-2 vector (Figure 1B). Similarly, the 29389–29751 nucleotide region (3'UTR) of SARS-CoV genomic sequence was PCR amplified and cloned into pCR-XL-TOPO vector to produce pCR-XL-TOPO-3'UTR (Figure 1B). The pCR-XL-TOPO-3'UTR was digested with *BamHI*, Klenow treated, and then digested by *EcoRV* and cloned into *SmaI* site in pIII MS2-1. All clones were checked by restriction mapping and sequencing.

Yeast Three-Hybrid Assay. The GAL-4 based yeast three-hybrid system (Figure 1D), kindly provided by Dr. M. Wickens (University of Wisconsin, Madison, WI) was used in the experiment (22). To prepare competent cells, L-40 strain was inoculated into 5 mL of YPD media and was grown on a 30 °C shaker at 200 rpm for 24 h. Next, 300 μ L of this culture was inoculated into 100 mL of YPD media and was grown on a 30 °C shaker at 200 rpm until A_{600} was 0.8. The culture was then centrifuged at 3000 rpm for 2 min at room temperature, and the pellet was washed with 10 mL of LiAc (0.1M). The pellet was resuspended in 1 mL of LiAc (0.1 M).

To transform into host yeast cells, appropriate fusion constructs (10 μ g) were mixed with 4 μ g of carrier DNA in a microcentrifuge tube. To this, 100 μ L of L-40 competent cells were added, and the mixture was kept for 5 min at room temperature. Next, 280 μ L of 50% PEG-3350 was added to the reaction mixture, and it was kept for 45 min at 30 °C. Next, 43 μ L of dimethyl sulfoxide (DMSO) was added and mixed by inversion. Then, a heat shock was given at 42 °C for 5 min. A pulse spin was given, and the pellet was washed with 500 μ L of sterile water. It was finally dissolved into 100 μ L of water and plated on YPD. The plates were kept at 30 °C for 3 days. Next, from each YPD plate, 10 individual colonies were streaked on LeuUraHis⁻ plates only or LeuUraHis⁻ plates containing 50 mM 3-amino-1,2,3-triazole (3-AT) and the plates were kept for 3 days at 30 °C. The filter β -gal assay was performed by streaking doubly transformed yeast colonies onto filter paper and allowing them to grow for 2 days on selection medium. Yeast cells were permeabilized by freezing yeast-impregnated filters in liquid nitrogen and thawing at room temperature. The filter was placed over a second filter that was presoaked in 0.1 M phosphate buffer (pH 7.0) containing 300 mg/mL *O*-nitrophenyl-D-galactoside (X-gal) and 0.27% β -mercaptoethanol. Filters were left for 2 days at 30 °C to develop a blue color, which indicated a positive RNA–protein interaction. β -Galactosidase expression levels were determined using *O*-nitrophenyl-D-galactoside (23–28). To perform liquid β -galactosidase assay, 1.5 mL of L-40 culture having an A_{600} = 0.8 was centrifuged at 13 000 rpm for 3 min and the pellet was washed with 1.5 mL of Z-buffer (60 mM Na₂HPO₄, 40 mM NaH₂PO₄, 10 mM KCl, 1 mM MgSO₄) having a pH value of 7. The pellet was finally dissolved in 300 μ L of Z-buffer. To permeabilize yeast cells, microcentrifuge tubes containing yeast pellet with Z-buffer were frozen in liquid nitrogen and thawed at room temperature. Next, 700 μ L of Z-buffer having 50 mM β -mercaptoethanol was added. To this, 160 μ L of *O*-nitrophenyl-D-galactoside (10 mg/mL, made in Z-buffer and along with 50 mM β -mercaptoethanol)

was added, and the mixture was kept at 30 °C till a yellow color developed in the mixture. Relative enzymatic activity was determined in three independent transformants from each group, and standard deviation was calculated. The samples were processed together and were incubated for the same length of time. To stop the reaction, 400 μ L of sodium carbonate (1 M) was added. Reaction tubes were centrifuged at 13 000 rpm for 10 min, and the supernatant was transferred to cuvettes to calculate β -gal expression levels, which were determined by measuring A_{420} (26, 29, 30).

Protein Expression and Immunoprecipitation. The full-length 3a protein (pGAD-3a encoding 275 amino acids of 3a with N-terminal HA tag) and its deletion mutants (Table 1) were expressed in separate reactions using the in vitro coupled transcription–translation rabbit reticulocyte lysate (TNT) system (Promega, Madison, WI). The reaction was assembled according to the manufacturer's protocol. In parallel, one control reaction with an empty pGAD vector was also assembled and labeled as mock lysate. All reactions were then incubated for 90 min at 30 °C. Protein either was labeled with S³⁵ or was unlabeled. The expression of unlabeled protein was detected by immunoprecipitation followed by chemiluminescence (20X LumiGLO Reagent, cell signaling). For immunoprecipitation, a 10 μ L aliquot of the reaction products was incubated with 1 μ g of anti-HA antibody in 500 μ L of PBS (pH 7.0) and kept overnight on a rocking shaker at 4 °C. The next day, 100 μ L of 10% protein-A sepharose beads (Amersham, Buckinghamshire, U.K.) was added to the reaction and the reaction mix was kept on a rocking shaker for 90 min at 4 °C. The beads were then washed thrice with PBS (pH 7.0), resuspended in 10 μ L of SDS PAGE loading buffer (50 mM Tris-HCl pH 6.8, 5% β -mercaptoethanol, 2% SDS, 0.1% bromo-phenol blue, and 10% glycerol), and boiled. The supernatant was subjected to SDS PAGE, and the protein expression was analyzed either by autoradiography for labeled protein or by chemiluminescence for the unlabeled protein (30). Chemiluminescence was performed using 20X LumiGLO Reagent (cell signaling) as per the manufacturer's protocol.

Gel Shift Assay (EMSA). pCR-XL-TOPO-5'UTR and pCR-XL-TOPO-3'UTR were linearized by *HindIII* and used to transcribe ³²P labeled RNA using the T7 Maxi-script kit (Ambion, Austin, TX) and were purified using the RNeasy kit (Qiagen, Valencia, CA). Integrity of RNA transcripts was checked on a 6% urea–acrylamide gel. Unlabeled full-length 3a protein and its deletions were produced using the in vitro coupled transcription–translation rabbit reticulocyte system (Promega, Madison, WI) and verified by immunoprecipitation using anti-HA antibody.

To perform EMSA, unlabeled 3a protein and its deletion mutants or mock translated lysate were mixed with 75 000 cpm of ³²P labeled RNA and 25 μ g of yeast t-RNA, and the reaction was incubated on ice for 20 min in 20 μ L of binding buffer having 10 mM Tris-HCl (pH 7.5), 50 mM KCl, 1 mM DTT, and 10% glycerol. Reaction products were analyzed on native 6% polyacrylamide gel followed by autoradiography.

A supershift assay was performed by adding 1 μ g of anti-HA antibody in addition to the reaction mix used for EMSA. All other steps involved were exactly similar as described for EMSA. As a control for supershift assay, a nonspecific antibody was used.

For competition binding assay, unlabeled RNA was transcribed using Ambion's T7 Maxi script kit and checked on formaldehyde-agarose gel (data not shown). A 50-fold excess of unlabeled RNA was incubated along with the regular reaction mix, and gel shift assay was performed as described above (30).

UV-Cross-Linking Assay. Here, we have used immunoprecipitated 3a protein in order to reduce the background in the gel. To perform the UV-cross-linking assay, 15 μL of the unlabeled TNT reaction product was incubated with 1 μg of anti-HA antibody in 500 μL of PBS (pH 7.0) and kept overnight at 4 °C with gentle rocking. Next, 100 μL of 10% protein-A sepharose beads (Amersham, Buckinghamshire, U.K.) was added to the reaction and the reaction mix was kept for 90 min at 4 °C on a rocking shaker. The beads were then washed five times with PBS (pH 7.0) and dissolved in 15 μL of binding buffer as described for the EMSA experiment above. To this reaction mix was added 75 000 cpm of ^{32}P labeled RNA and 25 μg of yeast t-RNA. The reactions were incubated at room temperature for 20 min and kept on ice, where they were irradiated for 20 min with UV light (254 nm) having energy value of 1200 $\mu\text{J}/\text{cm}^2$. Next, RNase A was added at a concentration of 1.25 $\mu\text{g}/\text{mL}$ to digest excess RNA and the reaction mixture was incubated at 37 °C for 60 min. The reaction product was separated on 15% SDS-PAGE and was analyzed by typhoon variable mode imager (Amersham, Buckinghamshire, U.K.).

RESULTS

3a Protein Interacts with the 5' End of SARS Genomic RNA. Since the 3a protein has been suggested to be a structural component of the SARS virus particle, we wished to check whether 3a also associated with the viral genomic RNA. To begin with, we tested the ability of the 3a protein to associate with the 5'- and 3'UTRs of the SARS-CoV genomic RNA. Our primary experimental setup involved testing the interactions of 3a with 5'UTR and 3'UTR of the SARS-CoV genome, using the yeast three-hybrid method (22, 30, 31). In the yeast three-hybrid assay, plasmid constructs expressing a fusion RNA and a fusion protein of interest are transformed into a genetically engineered host strain that bears HIS3 and lacZ reporter genes downstream of a GAL4 responsive promoter. In the co-transformed yeast cell, the fusion RNA molecule bridges the two-hybrid proteins, one containing a DNA-binding domain (BD) and the other containing a transcriptional GAL-4 activation domain (AD), to which the test protein is fused, in-frame, thus resulting in the transcriptional activation of HIS3 and lacZ reporter genes downstream of the BD (Figure 1D).

To study the interaction of the 3a protein with genomic RNA by the yeast three-hybrid system, we designed constructs fusing MS2-RNA with the 5'UTR (1–264 nt) and the 3'UTR (29389–29751 nt) of SARS-CoV (Figure 1A, 1B, and 1D, Table 1), so as to express fusion RNA transcripts in (L-40 coat) yeast cells (Table 1). The full-length 3a gene of the SARS-CoV was cloned in-frame with the Gal4 AD to express the AD-3a protein (Figure 1C) (26, 27, 29). Expression of the full-length, S³⁵ labeled 3a protein (tagged with an HA epitope at the N-terminus) in pGAD vector was performed using the in vitro coupled transcription-translation rabbit reticulocyte lysate (TNT) system, followed by

immunoprecipitation using anti-HA antibodies (Figure 2A). The 3a protein was found to correspond to the correct molecular size, i.e., approximately 35 kDa. The expression of unlabeled 3a protein was analyzed and confirmed by immunoprecipitation followed by chemiluminescence (data not shown).

The yeast L-40-coat host strain was systematically cotransformed with the AD-3a construct along with MS2-5' SARS or MS2-3' SARS or other control plasmids. Cotransformants were selected on LeuUra⁻ dropout medium and tested again for their ability to grow in LeuUraHis⁻ dropout media containing increasing concentrations of 3-AT. As a second marker to detect positive RNA-protein interactions, the cotransformants that showed positive on the LeuUraHis⁻+3-AT plates were assayed for β -galactosidase activity using *O*-nitrophenyl-D-galactoside as described in Experimental Procedures (24, 25, 28). Results of the yeast three-hybrid assay are summarized in Figure 2B. As expected, the host strain (L40-coat) as well as single transformants did not show any HIS3 or β -gal reporter activity. Similarly, cotransformants bearing empty vectors (MS2- + AD-) showed negative growth on LeuUraHis⁻ dropout media and β -galactosidase assays. As a positive control for the assay, cotransformants expressing the iron response element (pIII MS2-IRE) and iron regulatory protein (AD-IRP) were tested for their ability to grow on LeuUraHis⁻ dropout medium and assayed for β -galactosidase activity (22, 32, 33). These cells showed positive histidine prototrophy and produced a distinct blue color on the β -galactosidase filter and bright yellow color for the liquid β -galactosidase assays (Figure 2B). Further, the strength of interaction was measured by growing these cells in different concentrations of 3-AT, which is known to be a competitive inhibitor of the HIS3 protein, thus enhancing the stringency of selection (34). Interestingly, of the two genomic regions (5'UTR and 3'UTR) which were tested for their ability to associate with the 3a protein, only the 5'UTR showed histidine prototrophy as well as strong β -galactosidase activity. The interaction between 5'UTR and 3a protein appeared to be relatively stronger than the positive control as judged by liquid β -galactosidase assay (Figure 2B). In contrast, the 3'UTR did not show any significant reporter activity, further suggesting that the 5'UTR specifically associates with the 3a protein.

In order to confirm the results obtained from the yeast three-hybrid assay, we verified the ability of the 3a protein to bind to the 5'UTR of the SARS genome by electrophoretic mobility shift assay (EMSA) and further confirmed the same by conducting a UV-cross-linking assay as well. Radiolabeled transcripts were prepared as described in Experimental Procedures. The integrity of the purified ^{32}P labeled transcripts was then analyzed on a 6% urea-polyacrylamide gel (data not shown). Unlabeled 3a protein was produced in vitro and EMSA was performed as described in Experimental Procedures (30, 35). Reaction products were analyzed by electrophoresis on native 6% PAGE gel and visualized by autoradiography. As a control experiment, mock lysate was incubated along with the labeled probe in a similar manner to rule out any possible binding of endogenous protein from the in vitro coupled transcription-translation rabbit reticulocyte lysate system. Figure 2C shows the results of this control experiment where the 5'UTR transcript binds with the 3a protein showing a clear mobility shift (lane 3). In

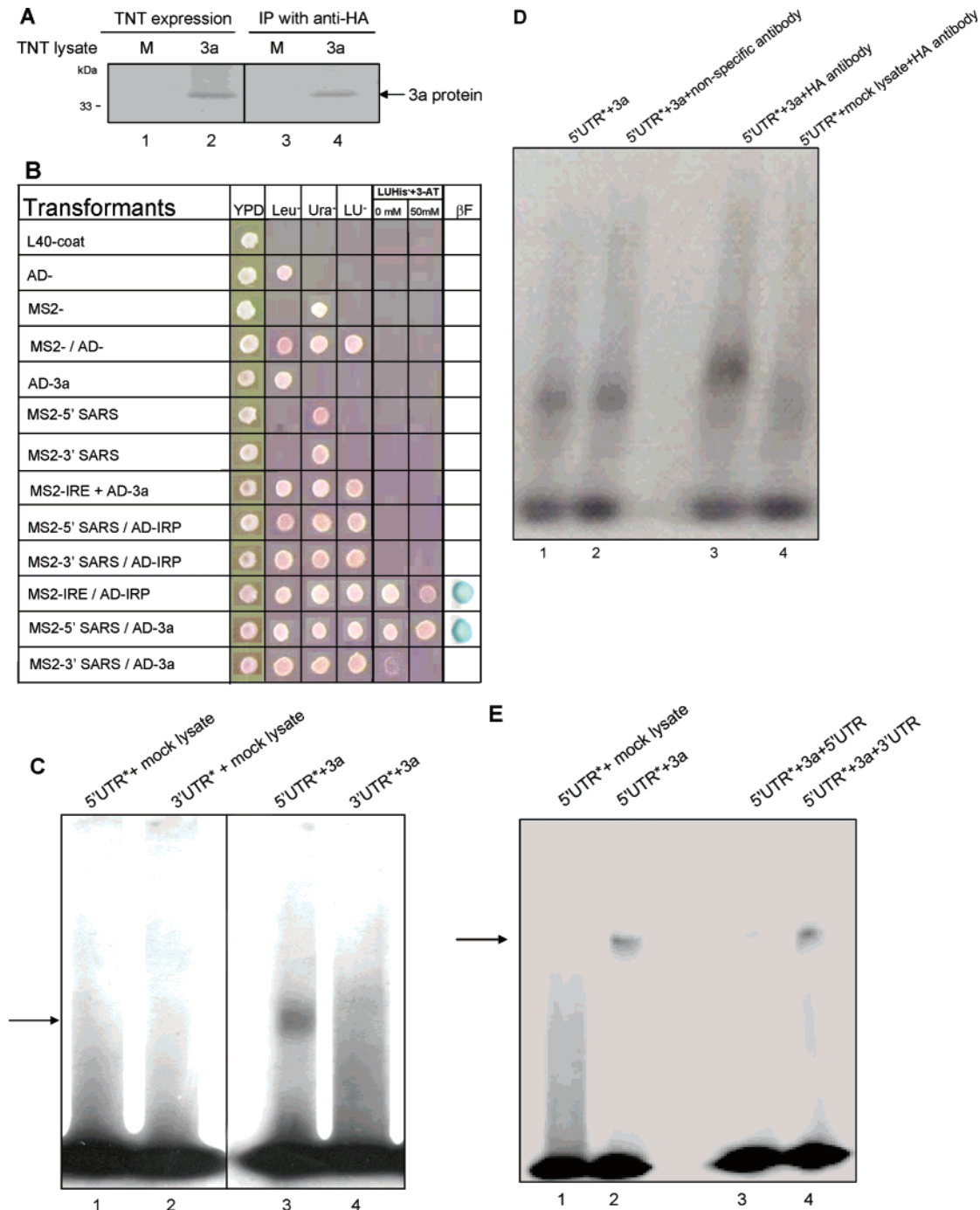


FIGURE 2: Full-length 3a protein interacts specifically with the 5'UTR. (A) The S^{35} labeled 3a protein tagged with an HA epitope was expressed in vitro using a rabbit reticulocyte coupled transcription–translation system (lane 2) and verified further by immunoprecipitation (lane 4) using anti-HA antibodies. The reaction mixtures were analyzed on a 15% SDS–polyacrylamide gel. Mock lysate was used as a negative control (lanes 1 and 3). The arrow shows 3a protein expression at approximately 35 kDa. M represents mock lysate. (B) Results from the three-hybrid analysis showing 5'UTR genomic RNA interacting with the 3a protein. YPD: yeast extract peptone dextrose media (nonselective). Leu⁻, Ura⁻, and LU⁻ represent SDLeu⁻ (synthetic dextrose complete media lacking leucine), SD-Ura⁻ (synthetic dextrose complete media lacking uracil), and SD-Leu⁻Ura⁻ (synthetic dextrose complete media lacking leucine and uracil); LUHis⁻+3-AT (synthetic dextrose complete media lacking histidine, leucine, and uracil with 3-aminotriazole) with 0 and 50 mM 3-aminotriazole (3-AT) added. βF represents results from the β-galactosidase filter assay. L40-coat is the untransformed yeast host strain. MS2-IRE/AD-IRP is used as a positive control in the assay (22, 33). (C) EMSA to verify the 3a-5'UTR interaction. The 5'UTR and 3'UTR were 32 P radiolabeled. Arrow shows the unlabeled 3a protein bound to 32 P labeled 5'UTR (lane 3) and not to 32 P labeled 3'UTR (lane 4). Lanes 1 and 2 are negative controls with mock translated lysate added to the reactions. * refers to 32 P labeled transcripts. (D) Supershift assay to confirm the results of mobility shift assay. The 5'UTR and 3'UTR were 32 P radiolabeled. Lane 3 shows the supershift observed by adding anti-HA antibody as compared to lane 1 where no antibody was added. As a control reaction, a nonspecific antibody was added instead of anti-HA antibody, and as expected, there was no supershift observed as shown in lane 2. Lane 4 shows a control reaction where mock lysate was added instead of 3a protein. The 3a protein being used in this experiment is unlabeled. * refers to 32 P labeled transcript. (E) Competitor binding assay to prove specificity of the RNA–protein interaction. The 3a protein being used in this experiment is unlabeled. Lane 4 contains a nonspecific competitor, 3'UTR RNA transcript. Lane 3 contains a 50-fold excess of unlabeled 5'UTR RNA transcript. Lanes 1 and 2 are negative and positive controls, respectively. * refers to 32 P labeled transcript. Non-radioactive transcripts 3'UTR and 5'UTR were used in 50-fold higher concentrations. Arrow shows 3a protein bound to 32 P radiolabeled 5'UTR.

contrast, the 5'UTR transcript incubated with the mock translated lysate (lane 1) or the 3'UTR transcript incubated with the mock lysate or lysate expressing the 3a protein (lane 2 and 4 respectively) all failed to show any shift in migration.

To finally prove that the mobility shift is a result of binding by the 3a protein, we performed a supershift assay where we added anti-HA antibody to the above reaction mix. The results of the supershift assay are shown in Figure 2D. A clear difference in mobility was observed for the complex having anti-HA antibody in addition to the 3a protein and 5'UTR (lane 3). Full-length 3a protein interacted with 5'UTR as a positive control (lane 1). A nonspecific antibody when used along with 3a and the 5'UTR showed negative supershift (lane 2), and a negative shift was also observed when the 3a protein was missing from the same reaction as in lane 3 (lane 4). This data, along with the mobility shift assay results, supports our hypothesis that the 5'UTR specifically associates with the 3a protein.

To further confirm the results of the gel-shift assay, a competitor-binding assay was performed. A 50-fold excess of the unlabeled 5'UTR transcript (specific competitor) was incubated along with the regular reaction mixture described above. Also, as a nonspecific competitor, unlabeled 3'UTR was used in 50-fold higher concentration in a parallel reaction. Results obtained from this experiment showed that the unlabeled 3'UTR did not compete for binding with the labeled 5'UTR–3a RNA–protein complex (Figure 2E, lane 4), whereas unlabeled 5'UTR was able to compete with the labeled probe for binding to the 3a protein, thus resulting in a significant decrease of the radioactive signal (Figure 2E, lane 3). Appropriate controls are shown in Figure 2E (negative, lane 1, and positive, lane 2).

Finally, we performed a UV–cross-linking assay to confirm the interaction of the 3a protein with the 5'UTR. The UV–cross-linking reaction was carried out as described in Experimental Procedures (36, 37). Results of the UV–cross-linking assay are shown in Figure 3A. Only the 5'UTR transcript was able to associate with the 3a protein (lane 4). As a control to show that the observed band was specific to the 3a protein, a parallel reaction was carried out containing mock translated lysate with the 5'UTR probe. As expected, no band corresponding to the size of the 3a protein was observed in this sample (lane 1). Further, the 3'UTR genomic region was unable to bind to the mock lysate or the 3a protein (lanes 2 and 3 respectively). These results henceforth confirmed our previous results obtained from the yeast three-hybrid assay and mobility shift assay (EMSA).

Next, a competitor-binding assay was also performed for the UV–cross-linking assay in a similar manner as described for EMSA. Again, a 50-fold excess of the unlabeled 5'UTR transcript (specific competitor) was incubated along with the regular reaction mixture described before and, as a nonspecific competitor, unlabeled 3'UTR was used in 50-fold higher concentration in a parallel reaction. As expected, unlabeled 3'UTR did not compete for binding with the labeled 5'UTR–3a RNA–protein complex (Figure 3B, lane 3), whereas unlabeled 5'UTR resulted in a significant disappearance of the radioactive signal (Figure 3B, lane 4). Appropriate controls are shown in Figure 3B (negative, lane 1, and positive, lane 2). These experiments clearly proved beyond doubt that the RNA–protein interaction was specific to the 5'UTR–3a protein of SARS-CoV.

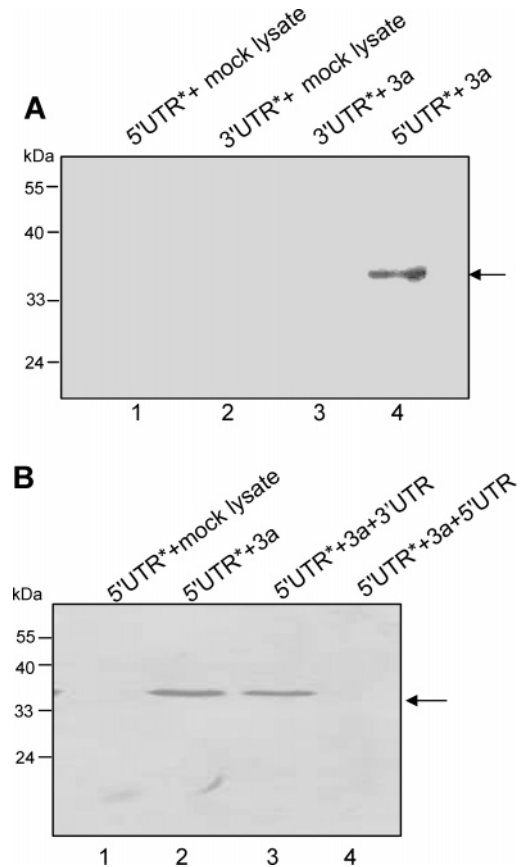


FIGURE 3: A UV–cross-linking assay to prove that the full-length 3a protein interacts specifically with 5'UTR of SARS-CoV. (A) A gel scanned by phosphorimager showing UV–cross-linking assay to verify the 3a–5'UTR interaction. The 3'UTR and 5'UTR were ^{32}P radiolabeled. A band was detected on a 15% SDS–polyacrylamide gel at approximately 35 kDa proving the interaction between unlabeled 3a and ^{32}P labeled 5'UTR (lane 4) whereas no interaction was seen for unlabeled 3a with ^{32}P labeled 3'UTR (lane 3). Lanes 1 and 2 are negative controls with mock translated lysate added to the reaction. * refers to ^{32}P labeled transcripts. Arrow shows the binding of 3a protein to labeled RNA. (B) UV–cross-linking competitor binding assay to prove specificity of the RNA–protein interaction. Lane 3 contains a nonspecific competitor, 3'UTR RNA transcript. Lane 4 contains a 50-fold excess of unlabeled 5'UTR of SARS-CoV RNA transcript. Lanes 1 and 2 are negative and positive controls, respectively. The 3a protein being used in this experiment is unlabeled. * refers to ^{32}P labeled transcript. The 3a protein has been shown by the arrow. Non-radioactive transcripts 3'UTR and 5'UTR were used in 50-fold higher concentrations.

Amino Acids 125–200 of the 3a Protein Constitute the Binding Domain Responsible for Interaction with the 5'UTR of the SARS-CoV RNA. We designed six deletion mutants of the 3a protein in an attempt to identify the region responsible for its RNA binding property. All 3a deletions were cloned in-frame with the Gal4 AD into the vector pGAD, as described in Table 1. Expression of various HA tagged deletion mutants of the 3a protein using a TNT kit were verified by immunoprecipitation using anti-HA antibodies followed by chemiluminescence (Figure 4A). Next, these deletions were used in a yeast three-hybrid assay to test for interaction with the 5'UTR region. Of the different mutant constructs, only AD-3a (125–275) and AD-3a (125–200) showed positive on the assay. AD-3a (1–70), AD-3a (1–124), AD-3a (70–124), and AD-3a (201–275) lost their ability to interact with the 5'UTR region (Figure 4B). As a nonspecific RNA control, 3'UTR was tested for interaction

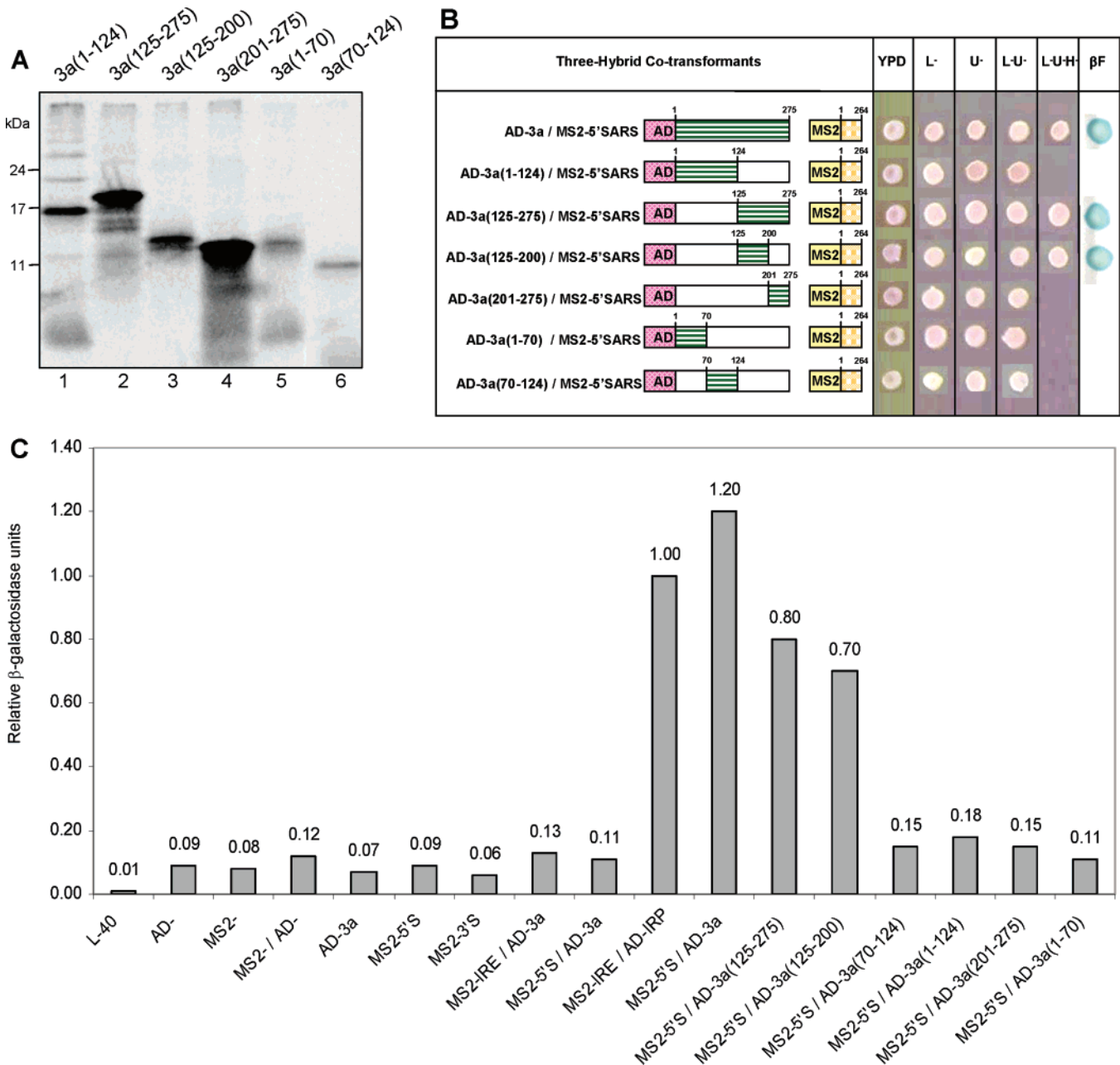


FIGURE 4: The RNA binding domain for 3a protein is present in the amino acid 125–200 region. (A) All deletions of the 3a protein were HA-tagged and expressed *in vitro* using a coupled transcription–translation system and further checked by immunoprecipitation using anti-HA antibodies followed by chemiluminescence. Result analysis was done on an 18% SDS–polyacrylamide gel. (B) Mapping the interaction domain for the 3a protein by yeast three-hybrid assay. Checkered boxes represent the AD region which was fused in-frame with the 3a protein and its deletions, shown in boxed regions filled with horizontal lines. Open boxes represent regions that were deleted from 3a. The numbers above the boxes fused with AD regions represent the first and last amino acid of the regions included in the 3a deletion constructs. The numbers above the boxes fused with MS2 regions represent the first and last nucleotide used to make the constructs (Table 1). Boxes filled with vertical lines represent the MS2 regions fused with the 1–264nt 5'UTR region from the SARS-CoV genome which is shown as boxes with squares. YPD: yeast extract peptone dextrose media (nonselective). L⁻ represents SD-Leu⁻; U⁻ represent SD-Ura⁻; LU⁻ represent SD-Leu⁻Ura⁻ synthetic growth media. L⁻U⁻H⁻ represents SD-Leu⁻Ura⁻His⁻ synthetic media. βF represents results from the β-galactosidase filter assay. (C) Comparison of interaction strengths of the 3a protein deletions using the yeast three-hybrid liquid β-galactosidase assay. The column graph represents relative β-galactosidase units from the liquid β-gal assay for interaction of both full-length 3a protein and its deletions, tested with 5'UTR of SARS-CoV. Standard deviation (not shown) was variable but did not exceed 25% of the experimental value. Values are given in arbitrary units. Relative β-galactosidase units for appropriate positive and negative controls are shown. S represents UTR of SARS-CoV here.

with all the 3a deletions, which gave negative results (data not shown). The three-hybrid analysis, thus, gave us a fairly good idea of the region of 3a imparting RNA binding activity to this protein.

In order to compare the relative strengths of interaction of the different 3a deletions with the 5'UTR, a liquid β-galactosidase assay was performed using yeast cells

cotransformed with 5'UTR and different 3a deletion constructs. Standard deviation (not shown) was variable but did not exceed 25% of the experimental value, as is typical for yeast two-hybrid experiments. Results of this experiment revealed that, of all the 3a deletions, only 3a (125–275) and 3a (125–200) showed significant β-galactosidase activity in the assay (Figure 4C). When compared, although less than

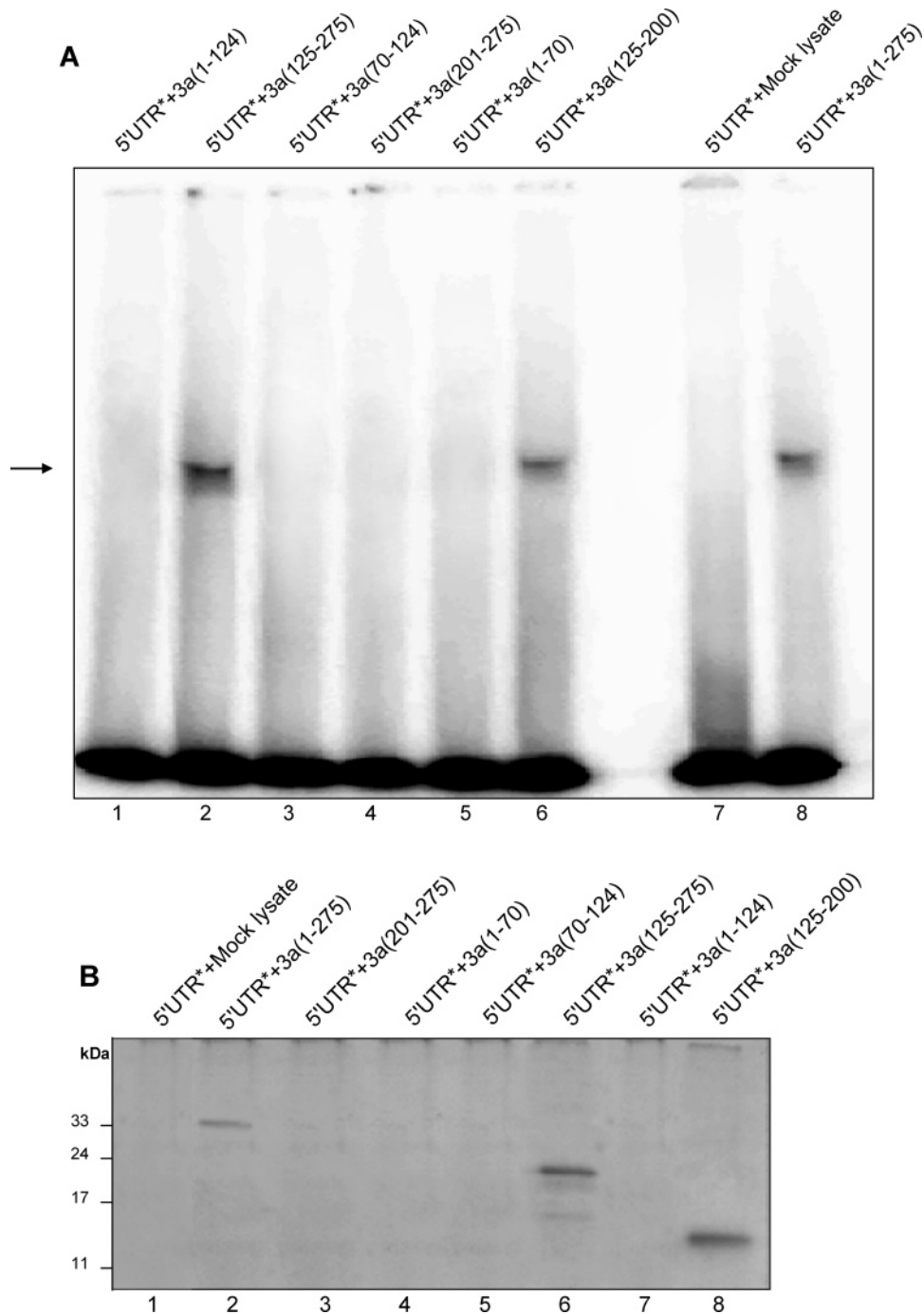


FIGURE 5: Mapping the interaction domain for the 3a protein. (A) EMSA showing that of all the deletion mutants of 3a, only 3a (125–275) and 3a (125–200) showed positive interaction with the 5'UTR region of SARS-CoV RNA (lanes 2 and 6, respectively). Arrow shows unlabeled protein bound to ^{32}P labeled RNA. Lanes 7 and 8 are negative and positive controls, respectively. * refers to ^{32}P labeled transcript. (B) UV-cross-linking assay to show the interaction domain for the 3a protein. A positive interaction with 5'UTR of SARS-CoV RNA was seen for 3a (125–200) and 3a (125–275) (lanes 8 and 6, respectively) when results were analyzed on a 15% SDS-polyacrylamide gel. All other deletion mutants proved negative by the assay. Lanes 1 and 2 represents negative and positive controls respectively. * refers to ^{32}P labeled transcript.

the full-length 3a protein, the relative β -galactosidase activity of 3a (125–200) interaction was found to be almost equal to that of 3a (125–275), indicating that these two deletion mutants were able to associate with 5'UTR, with equal efficiency. This data also suggests that deletion of the C-terminal 75 amino acids from the 3a (125–275) deletion does not adversely affect its RNA binding activity. Therefore, we propose that the 3a protein of SARS-CoV is capable of binding to the 5'UTR region of genomic RNA through its central 125–200 amino acid interaction domain.

Results obtained from the yeast three-hybrid system and liquid β -galactosidase assay were verified by EMSA. For this, all unlabeled 3a deletions were expressed in a coupled transcription-translation system. These unlabeled deletions were subsequently used for EMSA with ^{32}P radiolabeled 5'UTR transcript (Figure 5A). 5'UTR with full-length 3a protein was used as a positive control, and the 5'UTR with mock translated lysate served as a negative control for this experiment. Results thus obtained from this assay clearly showed that the full-length 3a (lane 8) as well its deletions

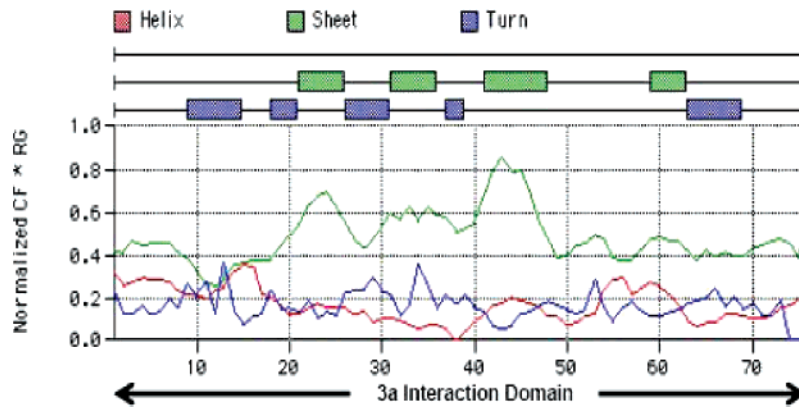


FIGURE 6: Predicted secondary structure of the RNA binding domain of 3a protein. The X-axis of the graph shows amino acid numbers of binding domain of 3a (75 amino acids long) whereas the Y-axis shows the normalized values obtained by using both Robson–Garnier and Chou–Fasman methods for helix, coil, and turn structures. This secondary structure plot has two parts: running average plot for the helix, coil, and turn structures; and structure prediction bars across the top of the plot. The CF and RG represent Chou–Fasman and Robson–Garnier.

3a (125–275) (lane 2) and 3a (125–200) (lane 6) were capable of interacting with the 5'UTR region of the SARS genome. These results fall in line with the yeast three-hybrid interaction domain mapping results.

To further validate the above observation, a UV–cross-linking assay was performed. Again, ^{32}P labeled 5'UTR transcript as well as all deletions of 3a used for this experiment were expressed and checked, as for EMSA. The cross-linking assay was performed using immunoprecipitated, unlabeled 3a protein as discussed before, along with appropriate controls (Figure 5B). Samples were resolved by SDS–PAGE, and bands were detected by phosphorimaging. As observed in Figure 5B, binding was detected only in the cases of full-length 3a (lane 2), 3a (125–275) (lane 6), and 3a (125–200) (lane 8). These results were in perfect agreement with our yeast three-hybrid assay and EMSA results.

DISCUSSION

This study uncovers the RNA binding activity of the 3a protein of SARS-CoV. All three assays, i.e., yeast three-hybrid, in vitro gel shift assays, and UV–cross-linking assays, showed a positive interaction between the 3a protein and the 5'UTR region of the SARS-CoV genome. The fact that the observed phenomenon was not an artifact of the experimental design was ruled out in multiple ways. First, the 3'UTR as well as the iron responsive element (IRE) containing RNA was unable to show any interaction with the 3a protein. Similarly, iron regulatory protein (IRP) was unable to interact with the 3'UTR or the 5'UTR, thus proving that the interaction between the 5'UTR and the 3a protein is a specific property exclusive to both partners. The RNA binding motif was mapped to the central 75 amino acids of the 3a protein. This region was found to consist of sheets and turns, when analyzed by Macvector program (Figure 6). The secondary structure plot shown in Figure 6 has two parts: running average plots for the helix, coil, and turn structures; and structure prediction bars across the top of the plot. Both Robson–Garnier and Chou–Fasman methods are used to construct this plot (38–43). A consensus plot has been generated using information from both Robson–Garnier and Chou–Fasman plots. The running average values are the products of the normalized values from each individual

plot, and structure prediction bars are only drawn where both methods agree. This region shares no homology with any known protein and hence may represent a novel RNA binding motif. Future studies using a mutagenesis approach will be useful in characterizing this motif.

Genomic RNA binding by viral proteins is a common phenomenon in RNA viruses. This serves two essential functions during the viral life cycle, viz., viral replication and packaging of the genome. Generally, the encapsidation signal in viruses is strategically placed such that only the full-length genome gets packaged into the viral capsid. In coronaviruses and many other RNA viruses, the nucleocapsid protein serves the function of binding the genomic RNA and encapsidating it. The genome incorporation signal in mouse hepatitis virus lies at about 20 kilobases from the 5'UTR (23). In some of the viruses like HIV, the responsibility of genome packaging is shared by more than one domain of a structural protein (44). In the case of mouse hepatitis virus, in addition to the nucleocapsid protein, another structural protein (M protein) has also been shown to cooperate in efficient full-length genome packaging although that cooperativity is mediated through the interaction of M with the nucleocapsid–RNA complex (45). These interactions may act as checkpoint mechanisms to enhance efficient genome packaging and prohibit incorporation of truncated or sub-genomic sequences. A contemporary work by Lu et al. has shown that 3a is a transmembrane protein (20). The probable explanation for accessibility of a transmembrane protein to RNA may be that either the 3a protein spans the membrane only once or, in addition to plasma membrane, it may also be localized at some other regions where it is accessible to RNA. Alternatively, the possibility of a transient RNA–protein interaction, where the protein is present in cytoplasm for a limited period of time which is enough for the interaction, cannot be ignored. As already discussed, the 3a protein has been shown to interact with spike, envelope, nucleocapsid, and membrane proteins (17). All these interactions, along with this new interaction, may form complexes that may prove as important players in viral assembly and/or viral release. An in vivo study needs to be performed on live virus to conclude the exact role of these interactions.

Since 3a has been shown to be a structural protein and is able to bind the 5'UTR of the genome, it appears to be an

attractive candidate that might cooperate with the nucleocapsid protein of the SARS-CoV during genome packaging. Additionally, as 5'UTR contains sequences required for replication, an alternative role of this interaction may be during replication. Moreover, a recent report has shown that, although deletion of the group-specific ORFs of SARS-CoV did not influence replication efficiency of virus to a significant level, the greatest reduction in virus growth occurred following ORF3a deletion (46). Thus, this interaction may be a significant component of the virus-replication machinery. If this is true, this interaction may, in the future, prove to be an important target for viral capsid assembly arrest or replication arrest.

ACKNOWLEDGMENT

Technical assistance by Purnima Kumar is gratefully acknowledged. Collaborative support from Microbiology Department, National University of Singapore, is gratefully acknowledged. We thank Dr. M. Wickens for the GAL-4 based yeast three-hybrid system. K.S. is a Senior Research Fellow of the University Grants Commission (UGC), India.

REFERENCES

- Marra, M. A., Jones, S. J., Astell, C. R., Holt, R. A., Brooks-Wilson, A., Butterfield, Y. S., Khattri, J., Asano, J. K., Barber, S. A., Chan, S. Y., Cloutier, A., Coughlin, S. M., Freeman, D., Gim, N., Griffith, O. L., Leach, S. R., Mayo, M., McDonald, H., Montgomery, S. B., Pandoh, P. K., Petrescu, A. S., Robertson, A. G., Schein, J. E., Siddiqui, A., Kabani, A., Li, Y., Normand, S., Yang, G. S., Plummer, F., Andonov, A., Artsob, H., Bastien, N., Bernard, K., Booth, T. F., Bowness, D., Czub, M., Drebot, M., Fernando, L., Flick, R., Garbutt, M., Gray, M., Grolla, A., Jones, S., Feldmann, H., Meyers, A., Kabani, A., Li, Y., Normand, S., Stroher, U., Tipples, G. A., Tyler, S., Vogrig, R., Ward, D., Watson, B., Brunham, R. C., Krajden, M., Petric, M., Skowronski, D. M., Upton, C., and Roper, R. L. (2003) The Genome sequence of the SARS-associated coronavirus, *Science* 300, 1399–1404.
- Rota, P. A., Oberste, M. S., Monroe, S. S., Nix, W. A., Campagnoli, R., Icenogle, J. P., Penaranda, S., Bankamp, B., Maher, K., Chen, M. H., Tong, S., Tamin, A., Lowe, L., Frace, M., DeRisi, J. L., Chen, Q., Wang, D., Erdman, D. D., Peret, T. C., Burns, C., Ksiazek, T. G., Rollin, P. E., Sanchez, A., Liffick, S., Holloway, B., Limor, J., McCaustland, K., Olsen-Rasmussen, M., Fouchier, R., Gunther, S., Osterhaus, A. D., Drosten, C., Pallansch, M. A., Anderson, L. J., and Bellini, W. J. (2003) Characterization of a novel coronavirus associated with severe acute respiratory syndrome, *Science* 300, 1394–1399.
- Shen, S., Lin, P. S., Chao, Y. C., Zhang, A., Yang, X., Lim, S. G., Hong, W., and Tan, Y. J. (2005) The severe acute respiratory syndrome coronavirus 3a is a novel structural protein, *Biochem. Biophys. Res. Commun.* 330, 286–292.
- Huang, C., Narayanan, K., Ito, N., Peters, C. J., and Makino, S. (2006) Severe acute respiratory syndrome coronavirus 3a protein is released in membranous structures from 3a protein-expressing cells and infected cells, *J. Virol.* 80, 210–217.
- Ruan, Y. J., Wei, C. L., Ee, A. L., Vega, V. B., Thoreau, H., Su, S. T., Chia, J. M., Ng, P., Chiu, K. P., Lim, L., Zhang, T., Peng, C. K., Lin, E. O., Lee, N. M., Yee, S. L., Ng, L. F., Chee, R. E., Stanton, L. W., Long, P. M., and Liu, E. T. (2003) Comparative full-length genome sequence analysis of 14 SARS coronavirus isolates and common mutations associated with putative origins of infection, *Lancet* 361, 1779–1785.
- Donnelly, C. A., Ghani, A. C., Leung, G. M., Hedley, A. J., Fraser, C., Riley, S., Abu-Raddad, L. J., Ho, L. M., Thach, T. Q., Chau, P., Chan, K. P., Lam, T. H., Tse, L. Y., Tsang, T., Liu, S. H., Kong, J. H., Lau, E. M., Ferguson, N. M., and Anderson, R. M. (2003) Epidemiological determinants of spread of causal agent of severe acute respiratory syndrome in Hong Kong, *Lancet* 361, 1761–1766.
- Ksiazek, T. G., Erdman, D., Goldsmith, C. S., Zaki, S. R., Peret, T., Emery, S., Tong, S., Urbani, C., Comer, J. A., Lim, W., Rollin, P. E., Dowell, S. F., Ling, A. E., Humphrey, C. D., Shieh, W. J., Guarner, J., Paddock, C. D., Rota, P., Fields, B., DeRisi, J., Yang, J. Y., Cox, N., Hughes, J. M., LeDuc, J. W., Bellini, W. J., and Anderson, L. J. (2003) A novel coronavirus associated with severe acute respiratory syndrome, *N. Engl. J. Med.* 348, 1953–1966.
- Eickmann, M., Becker, S., Klenk, H. D., Doerr, H. W., Stadler, K., Cesnini, S., Guidotti, S., Masignani, V., Scarselli, M., Mora, M., Donati, C., Han, J. H., Song, H. C., Abrignani, S., Covacci, A., and Rappuoli, R. (2003) Phylogeny of the SARS coronavirus, *Science* 302, 1504–1505.
- Gibbs, A. J., Gibbs, M. J., and Armstrong, J. S. (2004) The phylogeny of SARS coronavirus, *Arch. Virol.* 149, 621–624.
- Kim, O. J., Lee, D. H., and Lee, C. H. (2006) Close relationship between SARS-coronavirus and group 2 coronavirus, *J. Microbiol.* 44, 83–91.
- Snijder, E. J., Bredenbeek, P. J., Dobbe, J. C., Thiel, V., Ziebuhr, J., Poon, L. L., Guan, Y., Rozanov, M., Spaan, W. J., and Gorbalenya, A. E. (2003) Unique and conserved features of genome and proteome of SARS-coronavirus, an early split-off from the coronavirus group 2 lineage, *J. Mol. Biol.* 331, 991–1004.
- Geng, H., Liu, Y. M., Chan, W. S., Lo, A. W., Au, D. M., Wayne, M. M., and Ho, Y. Y. (2005) The putative protein 6 of the severe acute respiratory syndrome-associated coronavirus: expression and functional characterization, *FEBS Lett.* 579, 6763–6768.
- Ito, N., Mossel, E. C., Narayanan, K., Popov, V. L., Huang, C., Inoue, T., Peters, C. J., and Makino, S. (2005) Severe acute respiratory syndrome coronavirus 3a protein is a viral structural protein, *J. Virol.* 79, 3182–3186.
- Law, P. T., Wong, C. H., Au, T. C., Chuck, C. P., Kong, S. K., Chan, P. K., To, K. F., Lo, A. W., Chan, J. Y., Suen, Y. K., Chan, H. Y., Fung, K. P., Wayne, M. M., Sung, J. J., Lo, Y. M., and Tsui, S. K. (2005) The 3a protein of severe acute respiratory syndrome-associated coronavirus induces apoptosis in Vero E6 cells, *J. Gen. Virol.* 86, 1921–1930.
- Nelson, C. A., Pekosz, A., Lee, C. A., Diamond, M. S., and Fremont, D. H. (2005) Structure and intracellular targeting of the SARS-coronavirus Orf7a accessory protein, *Structure* 13, 75–85.
- Tan, Y. J., Fielding, B. C., Goh, P. Y., Shen, S., Tan, T. H., Lim, S. G., and Hong, W. (2004) Overexpression of 7a, a protein specifically encoded by the severe acute respiratory syndrome coronavirus, induces apoptosis via a caspase-dependent pathway, *J. Virol.* 78, 14043–14047.
- Tan, Y. J., Teng, E., Shen, S., Tan, T. H., Goh, P. Y., Fielding, B. C., Ooi, E. E., Tan, H. C., Lim, S. G., and Hong, W. (2004) A novel severe acute respiratory syndrome coronavirus protein, U274, is transported to the cell surface and undergoes endocytosis, *J. Virol.* 78, 6723–6734.
- Tan, Y. J. (2005) The Severe Acute Respiratory Syndrome (SARS)-coronavirus 3a protein may function as a modulator of the trafficking properties of the spike protein, *Virol. J.* 2, 5.
- Yu, C. J., Chen, Y. C., Hsiao, C. H., Kuo, T. C., Chang, S. C., Lu, C. Y., Wei, W. C., Lee, C. H., Huang, L. M., Chang, M. F., Ho, H. N., and Lee, F. J. (2004) Identification of a novel protein 3a from severe acute respiratory syndrome coronavirus, *FEBS Lett.* 565, 111–116.
- Lu, W., Zheng, B. J., Xu, K., Schwarz, W., Du, L., Wong, C. K., Chen, J., Duan, S., Deubel, V., and Sun, B. (2006) Severe acute respiratory syndrome-associated coronavirus 3a protein forms an ion channel and modulates virus release, *Proc. Natl. Acad. Sci. U.S.A.* 103, 12540–12545.
- Huang, Q., Yu, L., Petros, A. M., Gunasekera, A., Liu, Z., Xu, N., Hajduk, P., Mack, J., Fesik, S. W., and Olejniczak, E. T. (2004) Structure of the N-terminal RNA-binding domain of the SARS CoV nucleocapsid protein, *Biochemistry* 43, 6059–6063.
- SenGupta, D. J., Zhang, B., Kraemer, B., Pochart, P., Fields, S., and Wickens, M. (1996) A three-hybrid system to detect RNA-protein interactions in vivo, *Proc. Natl. Acad. Sci. U.S.A.* 93, 8496–8501.
- Fosmire, J. A., Hwang, K., and Makino, S. (1992) Identification and characterization of a coronavirus packaging signal, *J. Virol.* 66, 3522–3530.
- Guarente, L. (1983) Yeast promoters and lacZ fusions designed to study expression of cloned genes in yeast, *Methods Enzymol.* 101, 181–191.
- Tyagi, S., and Lal, S. K. (2000) Combined transformation and genetic technique verification of protein-protein interactions in

- the yeast two-hybrid system, *Biochem. Biophys. Res. Commun.* 277, 589–593.
26. Tyagi, S., Jameel, S., and Lal, S. K. (2001) Self-association and mapping of the interaction domain of hepatitis E virus ORF3 protein, *J. Virol.* 75, 2493–2498.
 27. Tyagi, S., Jameel, S., and Lal, S. K. (2001) A yeast two-hybrid study on self-association of the ORF2 protein of hepatitis E virus, *Biochem. Biophys. Res. Commun.* 284, 614–621.
 28. Tyagi, S., Salier, J. P., and Lal, S. K. (2002) The liver-specific human alpha(1)-microglobulin/bikunin precursor (AMBP) is capable of self-association, *Arch. Biochem. Biophys.* 399, 66–72.
 29. Tyagi, S., Korkaya, H., Zafrullah, M., Jameel, S., and Lal, S. K. (2002) The phosphorylated form of the ORF3 protein of hepatitis E virus interacts with its non-glycosylated form of the major capsid protein, ORF2, *J. Biol. Chem.* 277, 22759–22767.
 30. Surjit, M., Jameel, S., and Lal, S. K. (2004) The ORF2 protein of hepatitis E virus binds the 5' region of viral RNA, *J. Virol.* 78, 320–328.
 31. Srivastava, R., and Lal, S. K. (2002) A liquid synchronized-growth culture assay for the identification of true positive and negative yeast three-hybrid transformants, *Lett. Appl. Microbiol.* 34, 300–303.
 32. Rose, M. D., Winston, F., and Hieter, P. (1990) Methods in Yeast Genetics, in *Laboratory course manual*, Cold Spring Harbor Laboratory, Cold Spring Harbor, NY.
 33. Zhang, B., Gallegos, M., Puoti, A., Durkin, E., Fields, S., Kimble, J., and Wickens, M. P. (1997) A conserved RNA-binding protein that regulates sexual fates in the *C. elegans* hermaphrodite germ line, *Nature* 390, 477–484.
 34. Bernstein, D. S., Buter, N., Stumpf, C., and Wickens, M. (2002) Analyzing mRNA-protein complexes using a yeast three-hybrid system, *Methods* 26, 123–141.
 35. Martin, F., Schaller, A., Eglite, S., Schumperli, D., and Muller, B. (1997) The gene for histone RNA hairpin binding protein is located on human chromosome 4 and encodes a novel type of RNA binding protein, *EMBO J.* 16, 769–778.
 36. Nakazawa, F., Kannemeier, C., Shibamiya, A., Song, Y., Tzima, E., Schubert, U., Koyama, T., Niepmann, M., Trusheim, H., Engelmann, B., and Preissner, K. T. (2005) Extracellular RNA is a natural cofactor for the (auto-)activation of Factor VII-activating protease (FSAP), *Biochem. J.* 385, 831–838.
 37. Ochs, K., Zeller, A., Saleh, L., Bassili, G., Song, Y., Sonntag, A., and Niepmann, M. (2003) Impaired binding of standard initiation factors mediates poliovirus translation attenuation, *J. Virol.* 77, 115–122.
 38. Chou, P. Y., and Fasman, G. D. (1974) Conformational parameters for amino acids in helical, beta-sheet, and random coil regions calculated from proteins, *Biochemistry* 13, 211–222.
 39. Chou, P. Y., and Fasman, G. D. (1974) Prediction of protein conformation, *Biochemistry* 13, 222–245.
 40. Chou, P. Y., and Fasman, G. D. (1978) Empirical predictions of protein conformation, *Annu. Rev. Biochem.* 47, 251–276.
 41. Chou, P. Y., and Fasman, G. D. (1978) Prediction of the secondary structure of proteins from their amino acid sequence, *Adv. Enzymol. Relat. Areas Mol. Biol.* 47, 45–148.
 42. Garnier, J., Osguthorpe, D. J., and Robson, B. (1978) Analysis of the accuracy and implications of simple methods for predicting the secondary structure of globular proteins, *J. Mol. Biol.* 120, 97–120.
 43. Robson, B., and Suzuki, E. (1976) Conformational properties of amino acid residues in globular proteins, *J. Mol. Biol.* 107, 327–356.
 44. Poon, D. T., Li, G., and Aldovini, A. (1998) Nucleocapsid and matrix protein contributions to selective human immunodeficiency virus type 1 genomic RNA packaging, *J. Virol.* 72, 1983–1993.
 45. Narayanan, K., Maeda, A., Maeda, J., and Makino, S. (2000) Characterization of the coronavirus M protein and nucleocapsid interaction in infected cells, *J. Virol.* 74, 8127–8134.
 46. Yount, B., Roberts, R. S., Sims, A. C., Deming, D., Frieman, M. B., Sparks, J., Denison, M. R., Davis, N., and Baric, R. S. (2005) Severe acute respiratory syndrome coronavirus group-specific open reading frames encode nonessential functions for replication in cell cultures and mice, *J. Virol.* 79, 14909–14922.

BI062057P